Journal of CO2 Utilization 73 (2023) 102517

Contents lists available at ScienceDirect

Journal of CO2 Utilization

journal homepage: www.elsevier.com/locate/jcou

Fixed-bed CO_2 adsorption onto activated char from the pyrolysis of a non-recyclable plastic mixture from real urban residues

Ana Ligero *, Mónica Calero, M. Ángeles Martín-Lara, Gabriel Blázquez, Rafael R. Solís *, Antonio Pérez

Department of Chemical Engineering, University of Granada, 18074 Granada, Spain

ARTICLE INFO

Keywords:
Char
Plastic
Pyrolysis
CO_2
Adsorption
Fixed-bed
ANFIS

ABSTRACT

The potential use of activated char obtained from the pyrolysis of a mixture of non-recyclable plastics for the adsorption of CO_2 in fixed-bed columns has been explored. The rejected fraction of plastics collected in a municipal solid treatment plant was pyrolyzed and the resulting char residue was activated to develop a porous carbonaceous material. The dynamic behavior of CO_2 adsorption was assessed by the breakthrough curves obtained in continuous column tests. Among all the available models, the curves were successfully fitted to the dose-response model. The effect of adsorption temperature (15–45 ºC), the inlet CO_2 concentration (10–40 %, vol.), and the adsorbent length of the bed (loadings, 1–2 g) on the efficiency of the process was evaluated by the surface response methodology applying an adaptative neural fuzzy inference system (ANFIS). A temperature rise exerted a negative effect on the adsorption capacity due to the physisorption properties of the process, the fed CO_2 concentration displayed a positive effect and the fixed-bed length did not play a remarkable influence.

1. Introduction

Plastic polymers have turned into an essential item in current society since they are ubiquitously present in almost all human activities such as packaging, construction, agriculture, transport, textiles, and healthcare, among others [1]. However, the management of plastics has become a worldwide issue that requires urgent attention due to the negative environmental impact associated with their unsustainability. The vast majority of plastic polymers are non-biodegradable, display a very short lifetime, are produced in vast volumes, and are bound to be landfilled [2].

Plastic waste possesses high potential as a hydrocarbon source for the chemical industry. Chemical recycling via pyrolysis is gaining attention for those plastic fractions that cannot be submitted to a mechanical recycling process, due to its complexity or lack of interest [3], addressing moreover the challenges of plastic waste management. This scheme also promotes the development of the circular economy, feeding the vast majority of the materials within the 'loop' instead of the exploitation of new natural resources. Chemical recycling entails the conversion of end-of-life plastics into lower molecular weight products that can potentially be used as a feedstock in the production of new petrochemicals or even new polymers [4]. The conversion process involves the chemical transformation of the polymer structure into lighter fractions by the lysis action of the temperature [5]. Furthermore, the use of solid catalysts during the process can potentiate the yield of lighter fractions or improve the efficiency of diesel fuel [6].

The char yield in the pyrolysis of plastics is estimated at around 1–10 %, depending on the operational conditions [7], or the nature of the raw polymer [8]. Low temperatures and heating rates promote the formation of the char [9]. The char can be used as a fuel [10], an additive for epoxy composites with a previous functionalization [11,12], for asphalt binder [13], or as an adsorbent [14], with limited adsorption capacity. Upgraded properties have been reported for adsorption applications after activation of the char. Different activation methodologies based on physical or chemical agents have been applied to enhance the textural properties rising the surface area and microporosity [15] and boosting the adsorption capability of the activated char [16]. The resulting material has proved to be effective in the removal of heavy metals [17], aqueous organic pollutants [18,19], or gas purification [20,21].

The reduction in emissions of greenhouse gases is a paramount issue that must be addressed to reduce the consequences of climate change. Carbon capture and storage have been outlined as a plausible solution

* Corresponding authors.
E-mail addresses: aligero@correo.ugr.es (A. Ligero), mcaleroh@ugr.es (M. Calero), marianml@ugr.es (M.Á. Martín-Lara), gblazque@ugr.es (G. Blázquez), rafarsolis@ugr.es (R.R. Solís), aperezm@ugr.es (A. Pérez).

https://doi.org/10.1016/j.jcou.2023.102517
Received 18 April 2023; Received in revised form 7 June 2023; Accepted 11 June 2023
Available online 17 June 2023

for the reduction of CO_2, especially the release after post-combustion. There are some technical solutions such as absorption, membranes, cryogenics, adsorption onto solid materials, and calcium looping cycle. Although the amine absorption process is industrially mature, the corrosive properties of amine, their environmental impact, and the regeneration of the amine are energy-demanding and force the implementation of complex installations resistant to corrosion [22]. In this sense, adsorption outstands as a competitive alternative. Diverse highly porous materials have been researched as potential candidates for CO_2 adsorption such as carbonaceous materials [23], zeolites [24,25], and metal-organic frameworks [26] which are the most widely investigated to date. Carbon materials display low density and limited adsorption capacity which makes them less competitive than other more effective ones such as zeolites; however, their easy preparation, abundance, and low cost make them competitive at real large-scale applications. Moreover, the regeneration of the spent adsorbent after use, an aspect of paramount importance, can be carried out by temperature swing, pressure swing, or under vacuum conditions [27]. Furthermore, the combination of these strategies, i.e. temperature, and pressure, has been postulated as promising results [28].

This work provides a fixed-bed study of CO_2 adsorption using an activated char obtained from the pyrolysis of a rejected mixture of plastics not suitable for mechanical recycling. The residue of the pyrolysis, named char and poorly porous, was chemically activated with KOH to develop a microporous texture able to capture CO_2 by adsorption. In a previous work, the effect of the preparation method on the characteristics and CO_2 adsorption capacity of the char from the pyrolysis of mixed plastic waste was studied [29]. The char was activated using physical and chemical methods and adsorption tests were performed by thermogravimetric analysis. The highest CO_2 adsorption capacity achieved was 62 mg CO_2 g^{-1} using char activated with KOH and an operating temperature of 15 ºC. This work provides a continuation of the study, providing an analysis of dynamic tests in a continuous fixed-bed column, paying attention to the analysis of the breakthrough curves of the activated char. The influence of operational variables affecting the continuous adsorption of CO_2 such as temperature, inlet CO_2 concentration, and length of the bed was explored. A design of experiments and a modeling analysis by an adaptative neuro-fuzzy inference system (ANFIS) was carried out to optimize the operational conditions that maximize the CO_2 adsorption capacity and the removal percentage.

2. Experimental section

2.1. Preparation and activation of the char

The char was generated during the thermal pyrolysis of a non-recyclable mixture of plastics from the rejected fraction of plastics collected in the municipal solid waste treatment plant located in Alhendín, Granada (Spain). This plastic residue was composed of polypropylene (PP), polystyrene (PS), as high impact PS (HIPS) and expanded PS (EPS), and film, mainly made of polypropylene and polyethylene. The plastics were classified by polymer families leading to the following composition (mass percentages): PP (55 %), HIPS (8.6 %), EPS (10.1 %), and Film, (27.7 %). The mixture was crushed to a particle size lower than 1 mm.

The crushed mixture was submitted to pyrolysis in a tubular furnace under an N_2 flow (50 L h^{-1}) for 90 min, with an initial heating rate of 50 ºC min^{-1} and a holding temperature of 500 ºC. After, the residue solid obtained (approx. 6.2 % of initial mass) was ground. The obtained char was chemically activated with KOH based on previous work [29]. For the activation process, 5 g of char was mixed with KOH at char: KOH ratio of 2:1. The resulting mixture was heated under an N_2 atmosphere (200 mL min^{-1}) to 300 ºC, at a rate of 10 ºC min^{-1}. The temperature was kept for 1 h at 300 ºC leading to the melting of the KOH. Next, the temperature was risen to 760 ºC (heating rate, 10 ºC min^{-1}) and kept for 1 h. Finally, the sample was cooled down to room temperature. The resulting material was washed with HCl 1 M and water, dried (120 ºC, overnight), ground, and sieved to 250 μm.

Table 1
Characterization properties of the char before and after activation [29].

Technique	Parameter	Char	Activated char (AC)
Elemental analysis	N (%)	0.86	0.72
	C (%)	35.62	28.76
	H (%)	2.23	0.86
	O (%)*	15.08	3.98
Proximate analysis	Moisture (%)	3.10	2.48
	Volatile (%)	27.89	11.89
	Ash (%)	46.21	66.01
	Fixed carbon (%)	22.81	19.62
Textural analysis	S_{BET} (m^2 g^{-1})	14.7	487.0
	S_{MP} (m^2 g^{-1})	0.8	414.2
	V_T (cm^3 g^{-1})	0.025	0.300
	V_{MP} (cm^3 g^{-1})	-	0.180
	V_{MP}/V_T (%)	-	60.0

* Obtained as difference including ash. S_{BET}: total specific surface area by BET method; S_{MP}: micropore surface area; V_T: total pore volume; V_{MP}: micropore volume.

Table 1 shows the main physicochemical characteristics of the char and the activated material in terms of proximate analysis, elemental composition, and textural properties.

2.2. Breakthrough adsorption curves of CO_2

The fixed-bed adsorption tests of CO_2 were carried out in a glass column of 10 cm in length and 1.0 cm internal diameter. The temperature was controlled by the use of a cooler circulating through the annular space of the column. Glass balls were placed at both ends of the column to avoid sample fluidization. The activated carbon sample was loaded within 1–2 g and a mixture of N_2 and CO_2 (100 mL min^{-1}) at a desired concentration was passed through the column. The concentration of CO_2 leaving the column was continuously monitored with an infrared CO_2 sensor (NDIR Edinburgh Instruments Ltd.). The breakthrough curves were depicted as the temporal concentration at the outlet (C_t) normalized to the inlet (C_0), i.e. C_t/C_0.

The CO_2 adsorption capacity was determined as the area below the removed CO_2, that means the 1-C_t/C_0 curve, from the initial time until the saturation time (t_{sat}), defined this as the time in which C_{tsat}/C_0 = 0.95 [30]:

$$q_{CO_2} = \frac{\vartheta C_0 \int_0^{t_{sat}} \left(1 - \frac{C_t}{C_0}\right) dt}{m_{AC}} \quad (1)$$

where υ (L s^{-1}) means the volumetric flow rate, C_0 (mol L^{-1}) is the inlet CO_2 concentration and m_{AC} (g) stands for the loaded mass of adsorbent in the column.

The removal capacity (R) was calculated as the amount of CO_2 retained in the column concerning the total fed CO_2:

$$R = \frac{q_{CO_2} m_{AC}}{\vartheta C_0 t_{sat}} = \frac{\int_0^{t_{sat}} \left(1 - \frac{C_t}{C_0}\right) dt}{t_{sat}} \quad (2)$$

The breakthrough curves were fitted to classical breakthrough curves for fixed-bed adsorption. The Thomas model has been deeply used for the estimation of the adsorption capacity and the rate constant [31]. It assumes that the plug flow takes place in the fixed bed, that the external and internal diffusion limitations are negligible and that the adsorption process is described by a second-order reaction kinetics, leading to the following expression for the normalized temporal evolution of the outlet concentration (C_t/C_0):

$$\frac{C_t}{C_0} = \frac{1}{1 + \exp\left(k_T C_0 \left(\frac{q_0 m}{\vartheta C_0} - t\right)\right)} \quad (3)$$

where k_T (L mg^{-1} s^{-1}) stands for the Thomas rate constant; q_0 (mg g^{-1}) is equilibrium adsorption capacity; m (g) is the mass of the absorbent in the column; and υ (L s^{-1}) the inlet flow rate.

The Yoon–Nelson model considers that the rate of decrease in the probability of adsorption for each molecule is proportional to the probability of adsorption and the probability of breakthrough, leading to the equation [32]:

$$\frac{C_t}{C_0} = \frac{1}{1 + \exp(k_{YN}(\tau - t))} \quad (4)$$

where k_{YN} (s^{-1}) is the Yoon–Nelson rate constant independent of time and τ (s) is the time required to reach 50% breakthrough.

The Bohart-Adams model proposes that the adsorption process is not instantaneous and that the rate is proportional to the residual adsorption capacity of the adsorbent and the concentration of the adsorbate [33]. The equation to describe the temporal evolution of adsorbate concentration is:

$$\frac{C_t}{C_0} = \frac{1}{1 + \exp\left(k_{BA} C_0 \left(\frac{a_0 x}{u C_0} - t\right)\right)} \quad (5)$$

where k_{BA} (L mg^{-1} s^{-1}) is the Bohart-Adams rate constant; a_0 (mg L^{-1}) is the initially available adsorption capacity of the adsorbent; x (cm) is the bed height and u (cm s^{-1}) is the linear flow velocity.

The models of Thomas, Yoon-Nelson, and Bohart–Adams are equivalent in terms of their mathematical expressions. Thus, the terms $k_{BA}C_0$, $k_T C_0$, and k_{YN} have the identical dimension of reciprocal time (min^{-1}) leading to the following relationships [34]:

$$k_T C_0 = k_{YN} = k_{BA} C_0 \quad (6)$$

$$\tau = \frac{q_0 m}{\vartheta C_0} = \frac{a_0 x}{u C_0} \quad (7)$$

As a consequence, from a mathematical point of view, the breakthrough curves are coincident and only the parameter values defined by the initial adsorbate concentration differ in each model.

The Clark model is based on the mass-transfer concept in combination with the Freundlich isotherm, describing the plug-flow behavior in a fixed-bed column [35]:

$$\frac{C_t}{C_0} = \frac{1}{(1 + A\exp(-rt))^{\frac{1}{n-1}}} \quad (8)$$

where A (dimensionless) and r (s^{-1}) is the Clark model constant, and n (dimensionless) is the Freundlich constant which represents a measure of adsorption intensity.

The dose-response model is another example of a simplified model that fits better the breakthrough curves at low and high times as it provides an asymmetric prediction [36]:

$$\frac{C_t}{C_0} = 1 - \frac{1}{1 + (k_{DR} t)^{\alpha}} \quad (9)$$

where α (dimensionless) and k_{DR} (s^{-1}) are the dose-response parameters. The dose-response model represents a sigmoidal curve only when the parameter α is more than unity ($\alpha > 1$) and decides the slope of the regression function. Thus, the breakthrough curve becomes more symmetric with the increase in α. The constant k_{DR} is related to the throughput volume that produces a half-maximum response.

2.3. Optimization by experimental design and ANFIS Model

A three-level centered composite design (CCD) was carried out by selecting three variables: temperature (15, 30, and 45 °C), CO_2 inlet concentration (10 %, 25 %, and 40%, vol. obtained with mixtures of CO_2 and N_2), and activated carbon amount in the bed (1.0, 1.5 and 2.0 g). Table 2 shows the conditions of all the experiments taken.

Table 2
Experimental conditions of the CCD.

Exp. nº	C_0 (% CO_2, vol.)	T (°C)	m_{AC} (g)
1	40	45	2.0
2	40	45	1.0
3	40	15	2.0
4	40	15	1.0
5	40	30	1.5
6	10	45	1.0
7	10	15	2.0
8	10	15	1.0
9	10	45	2.0
10	10	30	1.5
11	25	30	1.5
12	25	45	1.5
13	25	15	1.5
14	25	30	2.0
15	25	30	1.0
16	25	30	1.5

The operating conditions were optimized by the surface response methodology considering an adaptative neuro-fuzzy inference system (ANFIS) selecting two response variables, the CO_2 adsorption capacity (q_{CO2}) and the percentage removed (R). The neuro-fuzzy model combines the advantages of fuzzy logic systems and neural networks for the prediction of responses by non-linear fitting [37,38]. It establishes a point as the central operating conditions and around it, a series of points within the maximum and minimum operating conditions. It is based on an equation with independent variables, the use of the rules, a constant, and a Gaussian dependency equation. The ANFIS equation is a mathematical expression that predicts the behavior of the response variable (Y) as a function of the independent variable [39]:

$$Y = \frac{\sum_{l=1}^{16} a_l FR_l}{\sum_{l=1}^{16} FR_l} \quad (10)$$

where a_l represents the constant parameters, one per variable and level. Furthermore, each $F{\cdot}R_l$ is the combination of levels (low, medium, and high) for each independent variable. The $F{\cdot}R_l$ term is a function of Gaussian function (μ) for the three independent variables (X_i) with three levels (low, medium, and high), which are defined as follows:

$$\mu_{low} = \exp\left(-0.5 \bullet \left(\frac{X - X_{low}}{L}\right)^2\right) \quad (11)$$

$$\mu_{medium} = \exp\left(-0.5 \bullet \left(\frac{X - X_{medium}}{L}\right)^2\right) \quad (12)$$

$$\mu_{high} = \exp\left(-0.5 \bullet \left(\frac{X - X_{high}}{L}\right)^2\right) \quad (13)$$

where L is the width of the associated Gaussian function distribution, and X_i is the value of each independent variable at the considered level.

The ANFIS model estimates the response variable with the following equation:

$$Y = \frac{a_1 FR_1 + \ldots + a_{16} FR_{12}}{FR_1 + \ldots + FR_{12}} \quad (14)$$

The calculations were conducted by using software with ANFIS calculation.

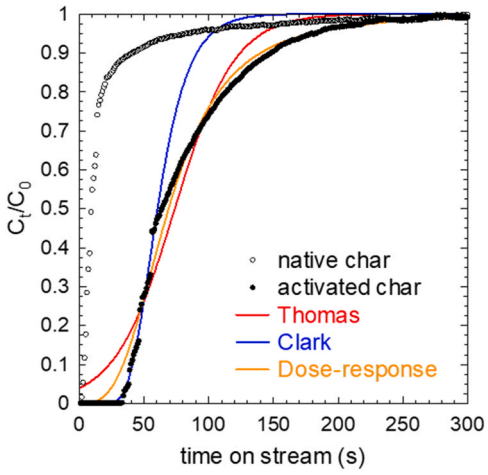

Fig. 1. Modeling fitting to the experimental CO_2 adsorption breakthrough. *Experimental conditions: T = 15 ℃, C_0= 10%; m_{AC}= 1 g.*

Table 3
Modeling fitting data results of CO_2 adsorption breakthrough. *Experimental conditions: T = 15 ℃, C_0= 10%; m_{AC}= 1 g.*

Model	Parameter	Value
Thomas	k_T (mL mg^{-1} s^{-1})	0.2329
	q_0 (mg g^{-1})	22.9
	Adj. R^2	0.974
Yoon-Nelson	k_{YN} (s^{-1})	0.0434
	τ (s)	73.8
	Adj. R^2	0.974
Bohart-Adams	k_{BA} (mL mg^{-1} s^{-1})	0.2329
	a_0 (mg L^{-1})	4515
	Adj. R^2	0.974
Clark	A	0.0489
	r (s^{-1})	0.0619
	N	1.0017
	Adj. R^2	0.927
Dose-response	k_{DR} (s^{-1})	0.0145
	α	3.0939
	Adj. R^2	0.994

3. Results and discussion

3.1. Modeling the breakthrough curves

The breakthrough curve of the CO_2 adsorption of the char before and after activation with KOH is depicted in Fig. 1. As it is illustrated, the native char immediately described the rise of the breakthrough curve from the beginning of the experiment, with a saturation time of 83 s, poorly retaining 6.2 mg CO_2 g^{-1} and removing 7.3 %. The activated char improved these results by delaying the appearance of CO_2 until 33 s, the saturation time appeared at 183 s, retaining 27.4 mg CO_2 g^{-1} and removing 26.1 %.

The experimental data were fitted to Thomas, Yoon-Nelson, Clark, and dose-response equations. The data were adjusted by non-linear regression techniques, using the adjusted determination coefficient (Adj. R^2) as the parameter to quantify the accuracy of the adjustment. Fig. 1 provides an example for the comparison of model suitability for the modeling of the breakthrough curves of CO_2 adsorption. Moreover, Table 3 provides the fitting results for the adjustment of the models. As can be appreciated, the model that best describes the evolution of the experimental data is the dose-response. The Yoon-Nelson model lacks confidence at low at high times of the curve. Although the Clark model fits well with the initial rise of the curve, at high times an important deviation is observed. The dose-response model due to the ability to describe asymmetric curves can predict with low error both parts of the

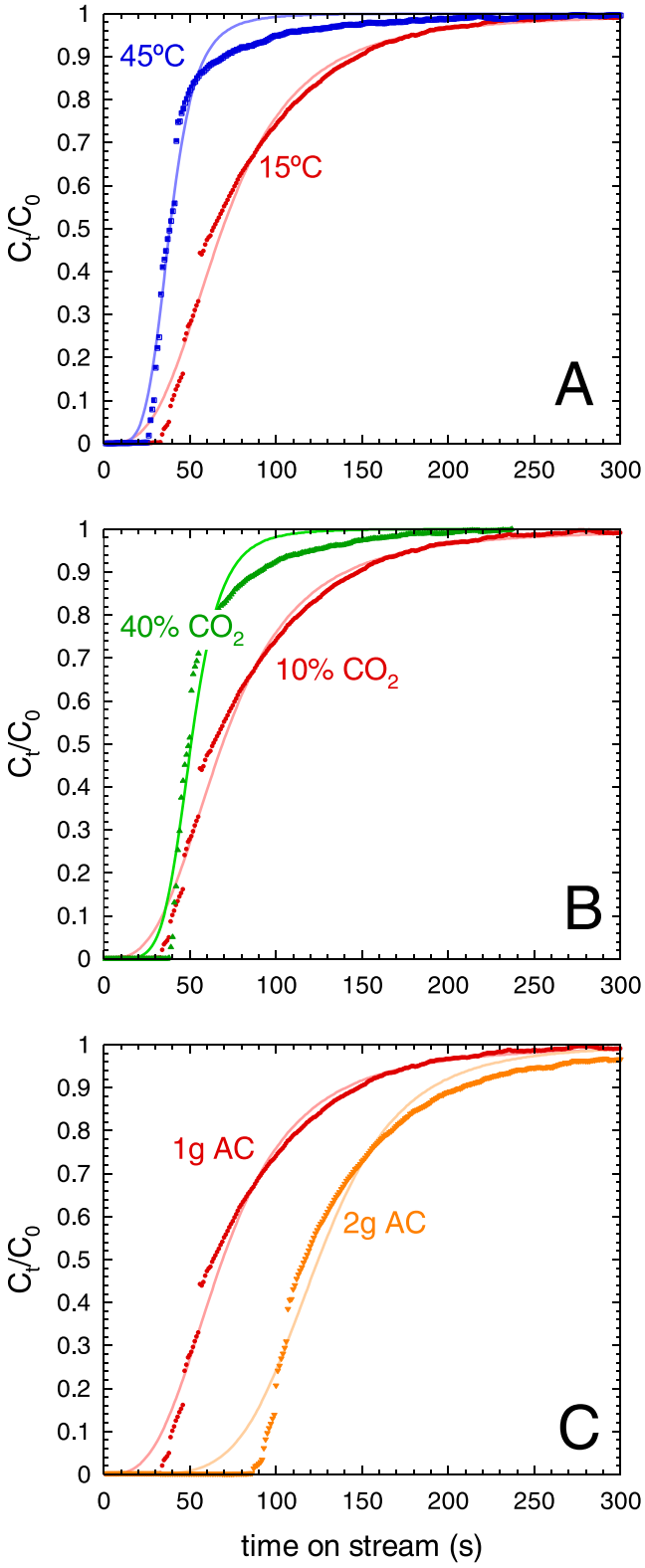

Fig. 2. Breakthrough curves of CO_2 adsorption. (A) Effect temperature (C_0 = 10 %; m_{AC}=1 g). (B) Effect of the inlet CO_2 concentration (T = 15 ℃, m_{AC}= 1 g). (C) Effect of the bed height (T = 15 ℃, C_0 =10 %). Lines: fitting to the dose-response model.

Table 4
Breakthrough parameters of the fixed-bed CO_2 adsorption and fitting to the dose-response model.

Exp. nº	Experimental conditions			Response variables			Fitting parameters to the Dose-response model		
	C_0 (% CO_2)	T (ºC)	m_{AC} (g)	q_{total} (mg CO_2)	q_{CO2} (mg CO_2 g^{-1})	R (%)	k_{DR} (s^{-1})	A	Adj. R^2
1	40	45	2.0	78.62	39.31	14.98	0.0195	9.5260	0.990
2	40	45	1.0	63.13	63.13	16.60	0.0257	7.3055	0.984
3	40	15	2.0	126.10	63.05	22.75	0.0119	8.6039	0.990
4	40	15	1.0	78.59	78,59	25.13	0.0197	5.8572	0.985
5	40	30	1.5	77.89	51.93	27.65	0.0192	9.2035	0.986
6	10	45	1.0	19.07	19.07	15.85	0.0260	5.1296	0.989
7	10	15	2.0	45.84	22.92	32.13	0.0080	5.1954	0.991
8	10	15	1.0	27.41	27.41	26.15	0.0145	3.0939	0.994
9	10	45	2.0	25.22	12.61	21.71	0.0152	5.8503	0.991
10	10	30	1.5	25.02	16.68	25.02	0.0152	6.1322	0.983
11	25	30	1.5	72.39	48.26	29.52	0.0166	5.8160	0.986
12	25	45	1.5	71.08	35.54	21.66	0.0193	4.5897	0.983
13	25	15	1.5	75.40	50.27	28.76	0.0122	6.9175	0.989
14	25	30	2.0	71.98	35.99	25.76	0.0130	9.0300	0.990
15	25	30	1.0	39.65	39.65	34.55	0.0216	4.6006	0.992
16	25	30	1.5	57.78	38.52	25.26	0.0163	6.5760	0.989

curve. Recently, some modifications of classical equations such as the Yoon-Nelson family [40] and Clark model [41] have been improved based on the fractal-like strategy in which the adsorption rate constant is considered time-dependent, enhancing considerably the fitting results. Nonetheless, this improvement in the fitting entails higher mathematical complexity, as one extra parameter in the equation is added. The dose-response model, a two-parameters model, was selected based on the good ability to replicate the experimental curve.

By contrast, as observed in Table 3, although the Thomas model does not reproduce the breakthrough curve very well, the adsorption capacity value predicted by the model is very similar to that obtained experimentally, 22.9 vs 27.4 mg g^{-1} respectively. Similarly, the Yoon-Nelson constant that represents the time when C_t/C_0 is equal to 0.5 ($\tau = 73.80$ s) coincides with that obtained experimentally, i.e. 63 s. Although in this study the dose-response is the model that best fits the whole shape of the breakthrough curve, Yoon-Nelson has been used to model the behavior of CO_2 over Zeolite 5 A in fixed-bed column [42].

3.2. Influence of the operational parameters

The influence of the three operational parameters, i.e. temperature, inlet CO_2 concentration, and fixed-bed length, which affect the process, is represented in Fig. 2. In addition, Table 4 shows the experimental results obtained in terms of q_{CO2} and R and the fitting parameters to the dose-response model.

Either temperature or the inlet CO_2 concentration affected the shape and breakthrough time of the adsorbent, see Fig. 2. At a fixed inlet CO_2 concentration and adsorbent mass, a temperature rise favors mass transfer, and, consequently, the concentration profile becomes steeper and the mass-transfer zone becomes narrower [43]. The adsorption capacity decreased with a temperature rise due to the exothermic nature of CO_2 adsorption [43,44]. Moreover, the CO_2 molecular diffusion increases with the temperature rise [45]. This fact provides evidence of the physisorption nature of the process [46], in which CO_2 and the functional groups of the activated char are weakened with temperature, and prone to be desorbed [47]. On the other side, if the temperature is kept constant and the inlet CO_2 increases, the CO_2 capacity considerably increases. This positive effect exerted by inlet CO_2 concentration is linked to a greater probability of several CO_2 molecules interacting with the active points of the adsorbent. Furthermore, the CO_2 concentration gradient is greater and consequently, the resistance to mass transfer is lowered [46,48]. This opposite effect of temperature and inlet CO_2 concentration is easily verified in extreme conditions. Fixing m_{AC}= 1 g for the fixed bed, the conditions with the best adsorption capacity were 40 % CO_2 and 15 ºC (78.59 mg CO_2 g^{-1}). On the contrary, the worst capacity was recorded at 10 % CO_2 and 45 ºC (19.07 mg CO_2 g^{-1}). This antagonism effect has also been reported in the CO_2 adsorption onto activated carbon from biomass origin [49].

The length of the fixed bed, represented by the adsorbent mass, as expected was translated in longer rupture times with no significant changes in the shape of the sigmoidal breakthrough curves, see Fig. 2C. The CO_2 capacity was within the same order, i.e. with 10 % of inlet CO_2 and 15 ºC, the adsorption capacities were 22.92 and 27.41 mg CO_2 g^{-1} for 1 and 2 g of adsorbent, respectively.

Several researchers have indicated similar behaviors in the study of the operating parameters in the adsorption of CO_2 with different adsorbent materials, using a fixed bed column. An increase in temperature produces a decrease in the adsorption forces and promotes desorption. Biochar obtained from marine algae activated with KOH was proved effective for the adsorption of CO_2, leading to an adsorption capacity decrease from 1.05 to 0.45 mmol g^{-1} (46.2–19.8 mg g^{-1}) for *Sargassum*-activated chars and 0.52–0.37 mmol g^{-1} (22.9–16.3 mg g^{-1}) for *Enteromorpha* activated chars when the temperature increased from 25 to 100 ºC [50]. Besides, this study reports that the adsorption capacities increased with the rise of the initial CO_2 concentration from 3 % to 18 %, varying from 0.23 to 1.08 mmol g^{-1} (10.1–47.5 mg g^{-1}) and from 0.13 to 0.56 mmol g^{-1} (5.7–24.6 mg g^{-1}) for the activated carbons prepared with *Sargassum* and *Enteromorpha*, respectively. This effect is associated with the higher mass transfer rate as the inlet CO_2 concentration rises. Another example of operating variables study during the adsorption of CO_2 in a fixed-bed column is represented by the use of natural yellow tuff [51]. The adsorption capacity was reported to decrease the temperature because, although with a temperature increase more energy is transmitted to the CO_2 molecules in the gas phase, making diffusion faster, the more excited CO_2 molecules are less likely to be trapped by the solid and the adsorbed CO_2 can escape from the attractive forces exerted by the adsorbent surface. The natural tuff led to, for example, for an initial concentration of 10 % CO_2, the adsorption capacity within 0.561 mmol g^{-1} at 25 ºC (24.7 mg g^{-1}) to a value of 0.124 mmol g^{-1} at 150 ºC (5.45 mg g^{-1}). The use of biochar obtained after hydrothermal carbonization of pineapple peel waste was found to be affected negatively by temperature in the capacity in a fixed-bed column, decreasing from 2.04 mmol g^{-1} (89.8 mg g^{-1}) to 1.25 mmol g^{-1} (55.0 mg g^{-1}) when the temperature raised from 30 to 70 ºC [52]. At higher temperatures, the adsorption equilibrium was reached faster due to the accelerated diffusion of CO_2 molecules in the pores of the adsorbent. Furthermore, as the temperature increased, the breakthrough times were found to decrease, indicating that the process was exothermic. In addition, the authors reported that as the initial concentration of CO_2 increased, the adsorption capacity increased, although the breakthrough and saturation times were shortened [52]. The effect of the feeding flow rate was also assessed, obtaining that with an

Table 5
Literature comparison of CO_2 uptake with carbon materials, zeolites, and MOFs.

Material		S_{BET} (m^2 g^{-1})	V_T (cm^3 g^{-1})	T (K)	q_{CO2} (mmol g^{-1})	Ref.
Carbon materials	Commercial GAC	954	0.48	298	1.66	[54]
	Commercial carbon nanotubes	394	0.91	298	1.57	[54]
	Graphene	620	0.71	298	2.28	[55]
	Graphene oxide	145	0.02	298	0.50	[56]
	Activated carbon from plastic char	487	0.30	298	1.79	This work
Zeolites	LTA	140	0.35	298	3.07	[57]
	Z4A	39	0.13	298	3.39	[58]
	5 A	334	0.18	298	3.68	[59]
	HZSM-5	373	0.29	298	4.11	[60]
	13X	876	0.35	298	6.18	[61]
MOFs	HKUST-1	1466	0.60	298	4.16	[62]
	MIL-125	1510	0.68	298	2.18	[63]
	NH_2-MIL-125	1492	0.60	298	4.00	[63]
	UiO-66	1390	0.70	273	2.20	[64]
	NH_2-UiO-66	1258	0.51	298	3.15	[65]
	NH_2-MIL-53(Al)	400	1.03	296	1.88	[66]
	FJU-90	1572	0.65	298	4.60	[67]
	MIL-101(Cr)	2166	1.07	298	1.17	[68]
	ZIF-8	880	0.46	298	0.67	[59]

The total pressure of the system in all the cases is 1 bar.

Table 6
Fitting constants to ANFIS model for adsorption capacity and removal percentage modeling.

Constant	q_{CO2} (mg g^{-1})	R (%)
a_1	24.15	28.26
a_2	32.32	21.74
a_3	44.68	18.29
a_4	25.32	10.39
a_5	13.08	36.15
a_6	22.45	52.19
a_7	25.95	40.51
a_8	21.08	34.75
a_9	17.98	84.74
a_{10}	29.84	66.12
a_{11}	16.93	67.24
a_{12}	13.55	38.76

increment of the flow rate from 30 to 70 mL min^{-1}, the adsorption capacity decreased from 2.04 to 1.55 mmol g^{-1} (89.8–68.2 mg g^{-1}) also reducing the breakthrough time from 6 to 2 min. At higher flow rates, shorter breakthrough times occur because of the retention and contact time between the gas molecules and the adsorbent surface, which were reduced [52]. A similar effect of the flow rate and temperature has also been obtained using other very different materials such as a molecular sieve and silica gel type-III [53] which suggest that the effect of the operating variables is related to the properties of CO_2 rather than the material used.

To assess the competitiveness of the prepared material, the adsorption capacity has been compared to other similar materials typically used for CO_2 capture and storage, see Table 5. The maximum value of 1.79 mmol CO_2 g^{-1} (40 % inlet CO_2, 15 ºC, 1 g material) was compared to other studies, including other remarkable carbonaceous materials, zeolites, and metal-organic frameworks (MOFs). Carbonaceous materials display a moderate CO_2 adsorption capacity, some modified graphene-based materials being the most promising in this group. Zeolites generally outstand as the most effective adsorbents, with uptakes over 3 mmol CO_2 g^{-1}. Metal-organic frameworks can be also very competitive if conveniently designed. However, regarding zeolites and especially in the case of the MOFs, their use at large-scale implies an important increase in the cost. The activated carbon prepared from the char pyrolysis of the plastic mixture displayed a similar CO_2 adsorption capacity if compared to commercial formulas, which confirms the suitability of the valorization of this char residue for the preparation of a competitive adsorbent.

Table 7
Parameters of the ANFIS model for the q_{CO2} and R modeling.

Variable	Level	q_{CO2}		R	
		X	L	X	L
Inlet CO_2 (%, vol.)	Low	11.100	13.600	10.000	6.370
	Medium	-	-	25.000	6.369
	High	42.310	9.839	40.000	6.370
Temperature (ºC)	Low	15.000	6.370	14.370	12.500
	Medium	30.000	6.370	-	-
	High	45.000	6.369	44.500	13.200
Adsorbent mass (g)	Low	0.874	0.213	0.874	0.233
	High	1.950	0.455	1.950	0.455

Table 8
Accuracy of ANFIS modeling to the adsorption capacity and removal percentage.

Exp. nº	q (mg g^{-1}), Adj. R^2= 0.983			R (%), Adj. R^2 = 0.969		
	q_{exp}	q_{calc}	q error (%)	R_{exp}	R_{calc}	R error (%)
1	39.31	39.59	0.73	14.98	15.29	2.11
2	63.13	63.22	0.15	16.60	16.61	0.09
3	63.05	63.26	0.34	22.75	22.59	0.68
4	78.59	78.63	0.06	25.13	25.12	0.01
5	51.93	51.37	1.08	27.65	28.01	1.30
6	19.07	19.07	0.03	15.85	15.85	0.04
7	22.92	22.63	1.23	32.13	31.86	0.84
8	27.41	27.40	0.02	26.15	26.13	0.07
9	12.61	12.29	2.53	21.71	22.58	4.02
10	16.68	17.30	3.74	25.02	25.89	3.51
11	48.26	41.38	14.24	29.52	26.50	10.20
12	35.54	34.59	2.66	21.66	20.37	5.94
13	50.27	49.44	1.64	28.76	29.10	1.20
14	35.99	41.46	15.20	25.76	26.31	2.15
15	39.65	39.91	0.68	34.55	34.49	0.15
16	38.52	41.38	7.44	25.26	26.50	4.94

3.3. Surface response curves by ANFIS model

The ANFIS model was applied to analyze the behavior of the operational parameters and explore the optimum conditions to maximize the CO_2 adsorption capacity and the removal percentage (R). The fitting constants of the ANFIS model are shown in Table 6, the parameters of the model regarding Eqs. 10 to 14 in Table 7, the accuracy is summarized in Table 8 and the surface response generated is illustrated in Fig. 3.

The ANFIS model applied was selected for two levels, high and low,

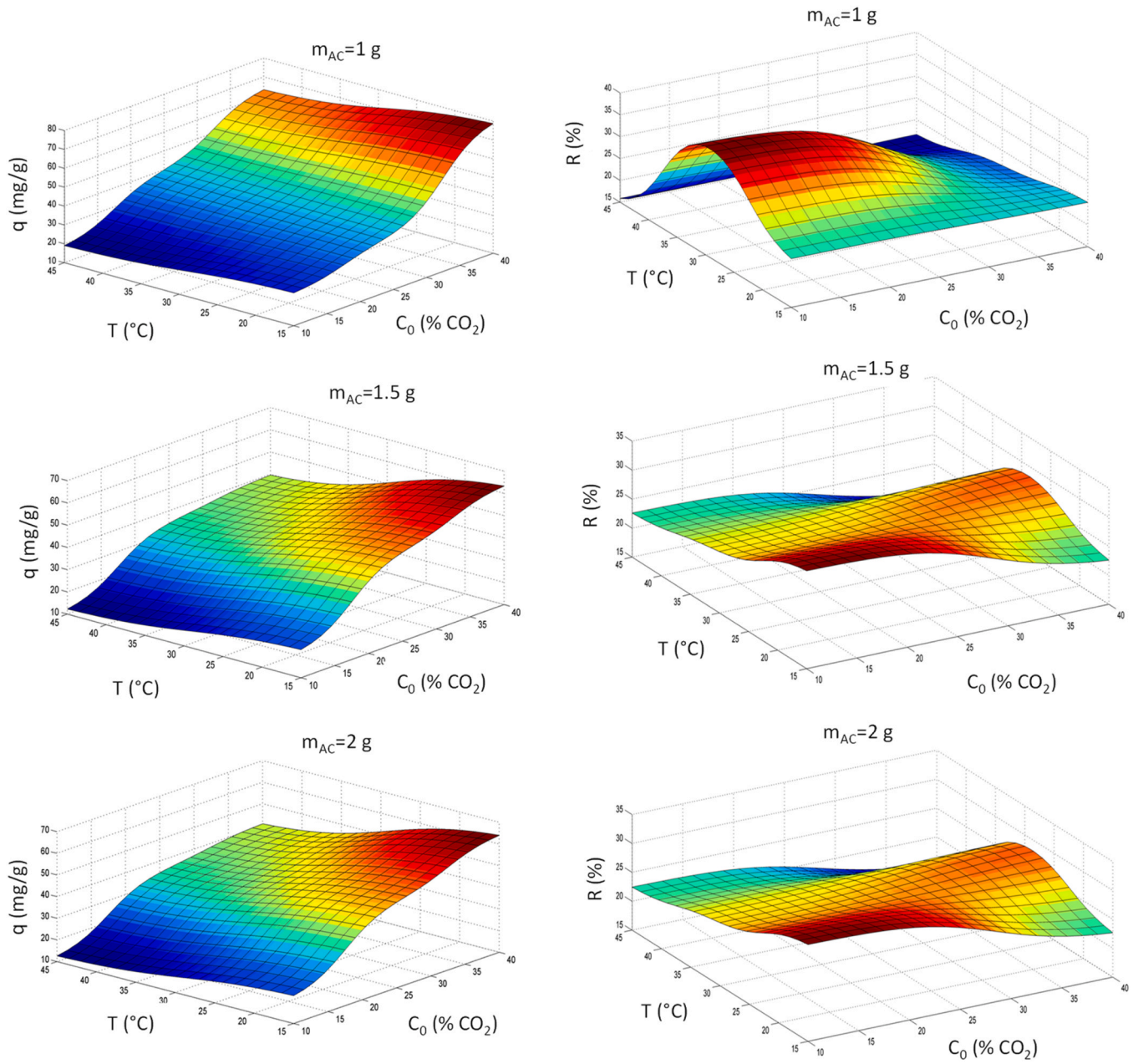

Fig. 3. Predicted surface response curves by ANFIS model for the adsorption capacity (q) and removal (R).

for the three variables (% CO_2, temperature, and adsorbent mass). An extra level, medium, was only added to one of the three variables due to the number of experiments conducted. The additional medium level was considered for the variables that affect the most to the response, i.e. inlet CO_2 concentration and temperature. Thus, as shown in Table 8 the best fitting results were acquired with the medium level in the temperature for the adsorption capacity and in the inlet CO_2 concentration for the removal as a response.

Table 8 also shows the experimental and calculated values and the relative error values for each studied response variable in all the experiments conducted. In general, the error between the model and the experimental data is lower than 5 %, and the Adj. R^2 for both responses, q_{CO2} and R, were > 0.9 The adjusted R^2 value was used as a tool to assess the goodness of the fitting model, leading to 0.983 and 0.969 in the modeling of the adsorption capacity and the removal percentage, respectively.

Fig. 3 corroborates that the higher the inlet CO_2 concentration and the lower the temperature, the adsorption capacity was maximized with no significant interaction between both variables. The presence of a maximum within the study range was appreciated at the highest adsorbate concentration and lowest temperature. The adsorbent loading in the column exerted a slightly negative effect, being the adsorbed capacity higher at the lower adsorbent load, i.e. the maximum CO_2 capacity was close to 80 mg g^{-1} (40 % CO_2, 15 ºC, m_{AC}= 1 g). This inverse dependence between CO_2 concentration and temperature with a lack of an optimum in a wider range has been also reported with biochar from softwood bark as adsorbent [69], with no boundary definition of the maximum CO_2 adsorbed within the range of study, leading to a predicted value of around 16.5 mg g^{-1} under C_0 = 40 % and T = 20 ºC. Very similar capacity adsorption (q_{CO2}=78 mg g^{-1}) was reported under similar operating conditions (35 % CO_2 inlet, T = 25 ºC) using as adsorbent biochar (white wood) after activation with KOH [70].

4. Conclusions

The char obtained as a residue in the chemical valorization of non-recyclable post-consumer plastics can be activated to develop an adsorbent with competitive properties for the adsorption of CO_2 in the gas phase. The adsorption process was studied in fixed-bed columns through the obtention of the breakthrough curves. The influence of inlet CO_2 concentration, temperature, and mass adsorbent in the bed was assessed, concluding that the two first are of paramount importance. The best result of CO_2 uptake was 78 mg g^{-1} under the highest inlet CO_2 (40 %), the lowest temperature (15 ºC), and moderate adsorbent load (1 g). The bed length displayed a minor influence. The ANFIS model was found as a useful tool to simulate the influence of the operational variables with a low deviation concerning the experimental data.

CRediT authorship contribution statement

Ana Ligero: Investigation, Methodology, Software, Writing – Original Draft; **Mónica Calero:** Investigation, Supervision, Writing – Review & Editing, Project Administration, Funding Acquisition; **María Ángeles Martín-Lara:** Investigation, Supervision, Writing – Review & Editing, Project Administration, Funding Acquisition; **Gabriel Blázquez:** Investigation, Supervision, Writing – Review & Editing; **Rafael R. Solís:** Investigation, Formal analysis, Writing – Original Draft, Visualization; **Antonio Pérez:** Conceptualization, Software, Supervision, Formal Analysis, Supervision, Writing – Review & Editing.

Declaration of Competing Interest

The authors declare that they have no known competing financial interests or personal relationships that could have appeared to influence the work reported in this paper.

Data Availability

Data will be made available on request.

Acknowledgments

This work has received funding from the project PID2019-108826RB-I00/SRA (State Research Agency)/10.13039/501100011033 and the project B-RNM-78-UGR20 (FEDER/Junta de Andalucía-Consejería de Transformación Económica, Industria, Conocimiento y Universidades).Funding for open access charge: Universidad de Granada/CBUA.

References

[1] A.M. Amadei, E. Sanyé-Mengual, S. Sala, Modeling the EU plastic footprint: exploring data sources and littering potential, Resour. Conserv. Recycl 178 (2022), 106086, https://doi.org/10.1016/J.RESCONREC.2021.106086.
[2] C.I. Idumah, I.C. Nwuzor, Novel trends in plastic waste management, Appl. Sci. 1 (2019) 1–14, https://doi.org/10.1007/S42452-019-1468-2.
[3] S.M. Al-Salem, P. Lettieri, J. Baeyens, Recycling and recovery routes of plastic solid waste (PSW): a review, Waste Manag. 29 (2009) 2625–2643, https://doi.org/10.1016/J.WASMAN.2009.06.004.
[4] O. Dogu, M. Pelucchi, R. Van de Vijver, P.H.M. Van Steenberge, D.R. D'hooge, A. Cuoci, M. Mehl, A. Frassoldati, T. Faravelli, K.M. Van Geem, The chemistry of chemical recycling of solid plastic waste via pyrolysis and gasification: state-of-the-art, challenges, and future directions, Prog. Energy Combust. Sci. 84 (2021), 100901, https://doi.org/10.1016/J.PECS.2020.100901.
[5] M.S. Qureshi, A. Oasmaa, H. Pihkola, I. Deviatkin, A. Tenhunen, J. Mannila, H. Minkkinen, M. Pohjakallio, J. Laine-Ylijoki, Pyrolysis of plastic waste: opportunities and challenges, J. Anal. Appl. Pyrolysis 152 (2020), 104804, https://doi.org/10.1016/J.JAAP.2020.104804.
[6] R. Miandad, M.A. Barakat, A.S. Aburiazaiza, M. Rehan, A.S. Nizami, Catalytic pyrolysis of plastic waste: a review, Process Saf. Environ. Prot. 102 (2016) 822–838, https://doi.org/10.1016/J.PSEP.2016.06.022.
[7] D.A. Wijesekara, P. Sargent, C.J. Ennis, D. Hughes, Prospects of using chars derived from mixed post waste plastic pyrolysis in civil engineering applications, J. Clean. Prod. 317 (2021), 128212, https://doi.org/10.1016/J.JCLEPRO.2021.128212.
[8] M.M. Harussani, S.M. Sapuan, U. Rashid, A. Khalina, R.A. Ilyas, Pyrolysis of polypropylene plastic waste into carbonaceous char: priority of plastic waste management amidst COVID-19 pandemic, Sci. Total Environ. 803 (2022), 149911, https://doi.org/10.1016/J.SCITOTENV.2021.149911.
[9] S.D. Anuar Sharuddin, F. Abnisa, W.M.A. Wan Daud, M.K. Aroua, A review on pyrolysis of plastic wastes, Energy Convers. Manag 115 (2016) 308–326, https://doi.org/10.1016/J.ENCONMAN.2016.02.037.
[10] J. Jamradloedluk, C. Lertsatitthanakorn, Characterization and utilization of char derived from fast pyrolysis of plastic wastes, Procedia Eng. 69 (2014) 1437–1442, https://doi.org/10.1016/J.PROENG.2014.03.139.
[11] S. Lee, Y.T. Kim, K.-Y.A. Lin, J. Lee, Plastic-waste-derived char as an additive for epoxy composite, Materials 16 (2023) 2602, https://doi.org/10.3390/MA16072602.
[12] M. Sogancioglu, E. Yel, G. Ahmetli, Pyrolysis of waste high density polyethylene (HDPE) and low density polyethylene (LDPE) plastics and production of epoxy composites with their pyrolysis chars, J. Clean. Prod. 165 (2017) 369–381, https://doi.org/10.1016/J.JCLEPRO.2017.07.157.
[13] A. Kumar, R. Choudhary, A. Kumar, Use of Char Derived from Waste Plastic Pyrolysis for Asphalt Binder Modification, in: International Conference on Innovative Technologies for Clean and Sustainable Development, Springer Science and Business Media B.V., 2021: pp. 337–356. https://doi.org/10.1007/978-3-030-51485-3_23.
[14] M.A. Martín-Lara, A. Piñar, A. Ligero, G. Blázquez, M. Calero, Characterization and use of char produced from pyrolysis of post-consumer mixed plastic waste, Water (Basel) 13 (2021) 1188, https://doi.org/10.3390/W13091188.
[15] I.P. da, P. Cansado, P.A.M. Mourão, J.M.V. Nabais, B. Tita, T. Batista, T. Rocha, C. Borges, G. Matos, Use of dirty plastic waste as precursors for activated carbon production—a contribution to the circular economy, Water Environ. J. 36 (2022) 96–104, https://doi.org/10.1111/WEJ.12762.
[16] R. Bhattacharya, A review on production and application of activated carbon from discarded plastics in the context of 'waste treats waste, J. Environ. Manag. 325 (2023), 116613, https://doi.org/10.1016/J.JENVMAN.2022.116613.
[17] R.R. Solís, M.Á. Martín-Lara, A. Ligero, J. Balbís, G. Blázquez, M. Calero, Revalorizing a pyrolytic char residue from post-consumer plastics into activated carbon for the adsorption of lead in water, Appl. Sci. 12 (2022) 8032, https://doi.org/10.3390/APP12168032.
[18] C. Lai, H. He, W. Xie, S. Fan, H. Huang, Y. Wang, B. Huang, X. Pan, Adsorption and photochemical capacity on 17α-ethinylestradiol by char produced in the thermo treatment process of plastic waste, J. Hazard. Mater. 423 (2022), 127066, https://doi.org/10.1016/J.JHAZMAT.2021.127066.
[19] P.J.M. Carrott, P.A.M. Mourão, M.M.L. Ribeiro Carrott, E.M. Gonçalves, Separating surface and solvent effects and the notion of critical adsorption energy in the adsorption of phenolic compounds by activated carbons, Langmuir 21 (2005) 11863–11869, https://doi.org/10.1021/LA0520886.
[20] S. Pérez-Huertas, M. Calero, A. Ligero, A. Pérez, K. Terpiłowski, M.A. Martín-Lara, On the use of plastic precursors for preparation of activated carbons and their evaluation in CO_2 capture for biogas upgrading: a review, Waste Manag. 161 (2023) 116–141, https://doi.org/10.1016/J.WASMAN.2023.02.022.
[21] B. Kaur, R.K. Gupta, H. Bhunia, Chemically activated nanoporous carbon adsorbents from waste plastic for CO_2 capture: breakthrough adsorption study, Microporous Mesoporous Mater. 282 (2019) 146–158, https://doi.org/10.1016/J.MICROMESO.2019.03.025.
[22] F. Raganati, F. Miccio, P. Ammendola, Adsorption of carbon dioxide for post-combustion capture: a review, Energy Fuels 35 (2021) 12845–12868, https://doi.org/10.1021/ACS.ENERGYFUELS.1C01618.
[23] X. Gao, S. Yang, L. Hu, S. Cai, L. Wu, S. Kawi, Carbonaceous materials as adsorbents for CO_2 capture: synthesis and modification, Carbon Capture Sci. Technol. 3 (2022), 100039, https://doi.org/10.1016/J.CCST.2022.100039.
[24] S. Kumar, R. Srivastava, J. Koh, Utilization of zeolites as CO_2 capturing agents: advances and future perspectives, J. CO_2 Util. 41 (2020), 101251, https://doi.org/10.1016/J.JCOU.2020.101251.
[25] V. Indira, K. Abhitha, A review on recent developments in Zeolite A synthesis for improved carbon dioxide capture: Implications for the water-energy nexus, Energy Nexus 7 (2022), 100095, https://doi.org/10.1016/J.NEXUS.2022.100095.
[26] Z. Li, P. Liu, C. Ou, X. Dong, Porous metal-organic frameworks for carbon dioxide adsorption and separation at low pressure, ACS Sustain. Chem. Eng. 8 (2020) 15378–15404, https://doi.org/10.1021/ACSSUSCHEMENG.0C05155.
[27] C. Dhoke, S. Cloete, S. Krishnamurthy, H. Seo, I. Luz, M. Soukri, Y. ki Park, R. Blom, S. Amini, A. Zaabout, Sorbents screening for post-combustion CO_2 capture via combined temperature and pressure swing adsorption, Chem. Eng. J. 380 (2020), 122201, https://doi.org/10.1016/J.CEJ.2019.122201.
[28] C. Dhoke, A. Zaabout, S. Cloete, S. Amini, Review on reactor configurations for adsorption-based CO_2 capture, Ind. Eng. Chem. Res 60 (2021) 3779–3798, https://doi.org/10.1021/ACS.IECR.0C04547.
[29] A. Ligero, M. Calero, A. Pérez, R.R. Solís, M.J. Muñoz-Batista, M.Á. Martín-Lara, Low-cost activated carbon from the pyrolysis of post-consumer plastic waste and the application in CO_2 capture, Process Saf. Environ. Prot. 173 (2023) 558–566, https://doi.org/10.1016/J.PSEP.2023.03.041.
[30] X. Wang, L. Chen, Q. Guo, Development of hybrid amine-functionalized MCM-41 sorbents for CO_2 capture, Chem. Eng. J. 260 (2015) 573–581, https://doi.org/10.1016/J.CEJ.2014.08.107.
[31] H.C. Thomas, Heterogeneous ion exchange in a flowing system, J. Am. Chem. Soc. 66 (1944) 1664–1666, https://doi.org/10.1021/JA01238A017.
[32] Y.H. Yoon, J.H. Nelson, Application of gas adsorption kinetics I. A theoretical model for respirator cartridge service life, Am. Ind. Hyg. Assoc. J. 45 (1984) 509–516, https://doi.org/10.1080/15298668491400197.

[33] G.S. Bohart, E.Q. Adams, Some aspects of the behavior of charcoal with respect to chlorine, J. Am. Chem. Soc. 42 (1920) 523–544, https://doi.org/10.1021/JA01448A018.
[34] Q. Hu, Y. Xie, C. Feng, Z. Zhang, Fractal-like kinetics of adsorption on heterogeneous surfaces in the fixed-bed column, Chem. Eng. J. 358 (2019) 1471–1478, https://doi.org/10.1016/J.CEJ.2018.10.165.
[35] R.M. Clark, Evaluating the cost and performance of field-scale granular activated carbon systems, Environ. Sci. Technol. 21 (1987) 573–580, https://doi.org/10.1021/ES00160A008.
[36] Q. Hu, Y. Xie, Z. Zhang, Modification of breakthrough models in a continuous-flow fixed-bed column: mathematical characteristics of breakthrough curves and rate profiles, Sep Purif. Technol. 238 (2020), 116399, https://doi.org/10.1016/J.SEPPUR.2019.116399.
[37] P.R. Souza, G.L. Dotto, N.P.G. Salau, Artificial neural network (ANN) and adaptive neuro-fuzzy interference system (ANFIS) modelling for nickel adsorption onto agro-wastes and commercial activated carbon, J. Environ. Chem. Eng. 6 (2018) 7152–7160, https://doi.org/10.1016/J.JECE.2018.11.013.
[38] J.S.R. Jang, ANFIS: adaptive-network-based fuzzy inference system, IEEE Trans. Syst. Man Cyber 23 (1993) 665–685, https://doi.org/10.1109/21.256541.
[39] G. Blázquez, M.Á. Martín-Lara, I. Iáñez-Rodríguez, I. Morales, A. Pérez, M. Calero, Cobalt biosorption in fixed-bed column using greenhouse crop residue as natural sorbent, Separations 9 (2022) 316, https://doi.org/10.3390/SEPARATIONS9100316/S1.
[40] Q. Hu, Y. Xie, C. Feng, Z. Zhang, Fractal-like kinetics of adsorption on heterogeneous surfaces in the fixed-bed column, Chem. Eng. J. 358 (2019) 1471–1478, https://doi.org/10.1016/J.CEJ.2018.10.165.
[41] Q. Hu, H. Liu, Z. Zhang, X. Pei, Development of fractal-like Clark model in a fixed-bed column, Sep Purif. Technol. 251 (2020), 117396, https://doi.org/10.1016/J.SEPPUR.2020.117396.
[42] A. Boonchuay, P. Worathanakul, The diffusion behavior of CO_2 adsorption from a CO_2/N_2 gas mixture on zeolite 5A in a fixed-bed column, Atmosphere 13 (2022) 513, https://doi.org/10.3390/ATMOS13040513.
[43] S. García, M.V. Gil, C.F. Martín, J.J. Pis, F. Rubiera, C. Pevida, Breakthrough adsorption study of a commercial activated carbon for pre-combustion CO_2 capture, Chem. Eng. J. 171 (2011) 549–556, https://doi.org/10.1016/J.CEJ.2011.04.027.
[44] M.S. Shafeeyan, W.M.A.W. Daud, A. Shamiri, N. Aghamohammadi, Modeling of carbon dioxide adsorption onto ammonia-modified activated carbon: kinetic analysis and breakthrough behavior, Energy Fuels 29 (2015) 6565–6577, https://doi.org/10.1021/ACS.ENERGYFUELS.5B00653.
[45] S. Shi, Y. Liu, Nitrogen-doped activated carbons derived from microalgae pyrolysis by-products by microwave/KOH activation for CO_2 adsorption, Fuel 306 (2021), 121762, https://doi.org/10.1016/J.FUEL.2021.121762.
[46] Y.L. Tan, M.A. Islam, M. Asif, B.H. Hameed, Adsorption of carbon dioxide by sodium hydroxide-modified granular coconut shell activated carbon in a fixed bed, Energy 77 (2014) 926–931, https://doi.org/10.1016/J.ENERGY.2014.09.079.
[47] C. Goel, H. Bhunia, P.K. Bajpai, Novel nitrogen enriched porous carbon adsorbents for CO_2 capture: breakthrough adsorption study, J. Environ. Chem. Eng. 4 (2016) 346–356, https://doi.org/10.1016/J.JECE.2015.11.017.
[48] R.J. Hook, An investigation of some sterically hindered amines as potential carbon dioxide scrubbing compounds, Ind. Eng. Chem. Res 36 (1997) 1779–1790, https://doi.org/10.1021/IE9605589.
[49] S. Shahkarami, R. Azargohar, A.K. Dalai, J. Soltan, Breakthrough CO_2 adsorption in bio-based activated carbons, J. Environ. Sci. 34 (2015) 68–76, https://doi.org/10.1016/J.JES.2015.03.008.
[50] S. Ding, Y. Liu, Adsorption of CO_2 from flue gas by novel seaweed-based KOH-activated porous biochars, Fuel 260 (2020), 116382, https://doi.org/10.1016/J.FUEL.2019.116382.
[51] P. Ammendola, F. Raganati, R. Chirone, F. Miccio, Fixed bed adsorption as affected by thermodynamics and kinetics: yellow tuff for CO_2 capture, Powder Technol. 373 (2020) 446–458, https://doi.org/10.1016/J.POWTEC.2020.06.075.
[52] M. Ibrahim, B.H. Hameed, A. Ouakouak, A.T.Mohd Din, Effect of hydrothermal carbonization parameters and performance of carbon dioxide adsorption on pineapple peel waste biochar, Chem. Eng. Technol. 45 (2022) 1982–1989, https://doi.org/10.1002/CEAT.202200089.
[53] M.K. Al Mesfer, M. Danish, M.I. Khan, I.H. Ali, M. Hasan, A. El Jery, Continuous fixed bed CO_2 adsorption: breakthrough, column efficiency, mass transfer zone, Processes 8 (2020) 1233, https://doi.org/10.3390/PR8101233.
[54] C. Lu, H. Bai, B. Wu, F. Su, J.F. Hwang, Comparative study of CO_2 capture by carbon nanotubes, activated carbons, and zeolites, Energy Fuels 22 (2008) 3050–3056, https://doi.org/10.1021/EF8000086.
[55] Y. Tian, Y. Lin, T. Hagio, Y.H. Hu, Surface-microporous graphene for CO_2 adsorption, Catal. Today 356 (2020) 514–518, https://doi.org/10.1016/J.CATTOD.2020.06.002.
[56] A. Pruna, A.C. Cárcel, A. Benedito, E. Giménez, Effect of synthesis conditions on CO_2 capture of ethylenediamine-modified graphene aerogels, Appl. Surf. Sci. 487 (2019) 228–235, https://doi.org/10.1016/J.APSUSC.2019.05.098.
[57] C. Chen, W.S. Ahn, CO_2 adsorption on LTA zeolites: effect of mesoporosity, Appl. Surf. Sci. 311 (2014) 107–109, https://doi.org/10.1016/J.APSUSC.2014.04.218.
[58] D. Panda, E.A. Kumar, S.K. Singh, Introducing mesoporosity in zeolite 4A bodies for rapid CO_2 capture, J. CO_2 Util. 40 (2020), 101223, https://doi.org/10.1016/J.JCOU.2020.101223.
[59] F. Gao, Y. Li, Z. Bian, J. Hu, H. Liu, Dynamic hydrophobic hindrance effect of zeolite@zeolitic imidazolate framework composites for CO_2 capture in the presence of water, J. Mater. Chem. A Mater. 3 (2015) 8091–8097, https://doi.org/10.1039/C4TA06645F.
[60] H. Cheng, H. Song, S. Toan, B. Wang, K.A.M. Gasem, M. Fan, F. Cheng, Experimental investigation of CO_2 adsorption and desorption on multi-type amines loaded HZSM-5 zeolites, Chem. Eng. J. 406 (2021), 126882, https://doi.org/10.1016/J.CEJ.2020.126882.
[61] C. Chen, D.W. Park, W.S. Ahn, CO_2 capture using zeolite 13X prepared from bentonite, Appl. Surf. Sci. 292 (2014) 63–67, https://doi.org/10.1016/J.APSUSC.2013.11.064.
[62] C. Chen, B. Li, L. Zhou, Z. Xia, N. Feng, J. Ding, L. Wang, H. Wan, G. Guan, Synthesis of hierarchically structured hybrid materials by controlled self-assembly of metal-organic framework with mesoporous silica for CO_2 adsorption, ACS Appl. Mater. Interfaces 9 (2017) 23060–23071, https://doi.org/10.1021/ACSAMI.7B08117.
[63] S.N. Kim, J. Kim, H.Y. Kim, H.Y. Cho, W.S. Ahn, Adsorption/catalytic properties of MIL-125 and NH_2-MIL-125, Catal. Today 204 (2013) 85–93, https://doi.org/10.1016/J.CATTOD.2012.08.014.
[64] C. Hon Lau, R. Babarao, M.R. Hill, A route to drastic increase of CO_2 uptake in Zr metal organic framework UiO-66, Chem. Commun. 49 (2013) 3634–3636, https://doi.org/10.1039/C3CC40470F.
[65] H. Molavi, A. Eskandari, A. Shojaei, S.A. Mousavi, Enhancing CO_2/N_2 adsorption selectivity via post-synthetic modification of NH_2-UiO-66(Zr, Microporous Mesoporous Mater. 257 (2018) 193–201, https://doi.org/10.1016/J.MICROMESO.2017.08.043.
[66] H.R. Abid, Z.H. Rada, X. Duan, H. Sun, S. Wang, Enhanced CO_2 adsorption and selectivity of CO_2/N_2 on amino-MIL-53(Al) synthesized by polar co-solvents, Energy Fuels 32 (2017) 4502–4510, https://doi.org/10.1021/ACS.ENERGYFUELS.7B03240.
[67] Y. Ye, Z. Ma, R.B. Lin, R. Krishna, W. Zhou, Q. Lin, Z. Zhang, S. Xiang, B. Chen, Pore space partition within a metal-organic framework for highly efficient C_2H_2/CO_2 separation, J. Am. Chem. Soc. 141 (2019) 4130–4136, https://doi.org/10.1021/JACS.9B00232.
[68] C. Chen, N. Feng, Q. Guo, Z. Li, X. Li, J. Ding, L. Wang, H. Wan, G. Guan, Template-directed fabrication of MIL-101(Cr)/mesoporous silica composite: layer-packed structure and enhanced performance for CO_2 capture, J. Colloid Interface Sci. 513 (2018) 891–902, https://doi.org/10.1016/J.JCIS.2017.12.014.
[69] H. Bamdad, K. Hawboldt, S. MacQuarrie, S. Papari, Application of biochar for acid gas removal: experimental and statistical analysis using CO_2, Environ. Sci. Pollut. Res. 26 (2019) 10902–10915, https://doi.org/10.1007/S11356-019-04509-3.
[70] S. Shahkarami, R. Azargohar, A.K. Dalai, J. Soltan, Breakthrough CO_2 adsorption in bio-based activated carbons, J. Environ. Sci. 34 (2015) 68–76, https://doi.org/10.1016/J.JES.2015.03.008.